The relationship between specific absorption rate and temperature elevation in anatomically based human body models for plane wave exposure from 30 MHz to 6 GHz

Akimasa Hirata, Ilkka Laakso, Takuya Oizumi, Ryuto Hanatani, Kwok Hung Chan, and Joe Wiart

1: Department of Computer Science and Engineering, Nagoya Institute of Technology, Japan
2: Orange Lab, France Telecom, France

Corresponding Author: Akimasa Hirata

Address: Nagoya Institute of Technology, Gokiso-cho, Showa-ku, Nagoya 466-8555, Japan

Tel&Fax: +81-52-735-7916

E-mail: ahirata@nitech.ac.jp

Abstract

According to the international safety guidelines/standard, the whole-body-averaged specific absorption rate (SAR) and the peak spatial average SAR are used as metrics for human protection from whole-body and localized exposures, respectively. The IEEE standard (2006) indicates that the upper boundary frequency, over which the whole-body-averaged SAR is deemed to be the basic restriction, has been reduced from 6 GHz to 3 GHz, because radio-wave energy is absorbed around the body surface when the frequency is increased. However, no quantitative discussion has been provided to support this description especially from the standpoint of temperature elevation. It is of interest to investigate the maximum temperature elevation in addition to the core temperature even for a whole-body exposure. In the present study, using anatomically based human models, we computed the SAR and the temperature elevation for a plane-wave exposure from 30 MHz to 6 GHz, taking into account the thermoregulatory response. As the primary result, we found that the ratio of the core temperature elevation to the whole-body-averaged SAR is almost frequency independent for frequencies below a few gigahertz; the ratio decreases above this frequency. At frequencies higher than a few gigahertz, core temperature elevation for the same whole-body averaged SAR becomes lower due to heat convection from the skin to air. This lower core temperature elevation is attributable to skin temperature elevation caused by the power absorption around the body surface. Then, core temperature elevation even for whole-body averaged SAR of 4 W kg^{-1} with the duration of 1 h was at most 0.8^{o}C, which is smaller than a threshold considered in the safety guidelines/standard. Further, the peak 10-g averaged SAR is correlated with the maximum body temperature elevations without extremities and pinna over the frequencies considered. These findings were confirmed for seven models, including models of a child and a pregnant female. Thus, the current basic restriction for whole-body exposure in the international guidelines is conservative. Peak spatial-averaged SAR can be used as a metric for estimating local temperature elevation even for whole-body exposure. Our computational results also support the description in the IEEE standard about the reduction of the upper applicable frequency of whole-body-averaged SAR from 6 GHz and 3 GHz; the power density reference level is more conservative than the basic restriction limit for the whole-body averaged SAR from the standpoint of temperature elevation.

1. Introduction

Elevated temperature (1–2°C) resulting from radio-frequency (RF) absorption is known to be a dominant cause of adverse health effects, such as heat exhaustion and heat stroke (ACGIH, 1996; Ziskin and Morrissey, 2011). In the International Commission on Non-Ionizing Radiation Protection (ICNIRP) guidelines (1998) and the IEEE standard (2006), the whole-body-averaged specific absorption rate (WBA-SAR) is used as a metric for human protection from RF whole-body exposure. In these guidelines, the basic restriction of WBA-SAR is 0.4 Wkg^{-1} for occupational exposure and 0.08 Wkg^{-1} for general public exposure. These thresholds are based on the fact that RF exposure of laboratory animals in excess of approximately 4 Wkg^{-1} has revealed a characteristic pattern of thermoregulatory responses (ICNIRP, 1998). Note that this approximate threshold was estimated from the experiment in 1980s (Michaelson, 1983).

For RF localized exposures, the peak value of SAR averaged over 10 g of tissue is used as a metric. The limit is 10 W kg^{-1} for occupational exposure and 2 W kg^{-1} for the general public exposure. However, the upper frequency where the SAR limits are imposed is different in the international guidelines/standard. In particular, the upper frequencies for WBA- and local SARs are both 10 GHz in the ICNIRP guidelines (1998) and 3 GHz and 6 GHz, respectively, in the IEEE standard (2006). According to the IEEE standard (2006), the upper boundary frequency over which the WBA-SAR is deemed to be the basic restriction has been reduced from 6 GHz to 3 GHz because RF energy is absorbed around the body surface with the increase of the frequency. However, the quantitative discussion provided is insufficient to support this description. It is of interest to investigate the local maximum temperature elevation in addition to the core temperature even for whole-body exposure.

Thermal dosimetry for RF whole-body exposure in humans was conducted computationally (Bernardi *et al.*, 2003; Foster and Adair, 2004; Hirata *et al.*, 2007a; Bakker *et al.*, 2011; Laakso and Hirata, 2011). Some previous studies took into account the thermophysiological response caused by the temperature elevation (Bernardi *et al.*, 2003; Foster and Adair, 2004; Hirata *et al.*, 2007a; Bakker *et al.*, 2011; Laakso and Hirata, 2011). In addition, an analytical formula to estimate the core temperature elevation has been proposed by Hirata *et al.* (2009). Then, a good correlation between the WBA-SAR and the core temperature elevations was shown for frequencies between 30 MHz and 2 GHz. Bakker *et al.* (2011) investigated the local SAR and the temperature elevation in the human bodies exposed at the allowable incident power density or reference level as specified by the ICNIRP guidelines for frequencies from 10 MHz to 5.6 GHz. The averaging volume considered was a cube. However, the thermophysiological response of humans was not taken into account, assuming that the core temperature was sufficiently small (Hirata *et al.*, 2008a). Laakso and Hirata (2011) investigated the dominant factors affecting the local and the core temperature elevations in a Japanese adult male model at the whole-body

resonance frequency and at 2 GHz.

In this study, local/whole-body SARs and local/core temperature elevations in human body models were investigated at frequencies from 30 MHz to 6 GHz. Then, we discussed the relationship between SARs and temperature elevations to clarify the rationale for the limits prescribed in the international standard/guidelines. The averaging schemes for local SAR prescribed in the IEEE standard and ICNIRP guidelines were considered.

2. Models and Methods

2.1. Human Body Models

In order to discuss the variability of the SAR and the temperature elevation caused by the model morphology, seven models were considered, including Japanese male and female models named TARO and HANAKO, respectively, (Nagaoka *et al.*, 2004) and a three-year-old child model developed on the basis of TARO (Nagaoka *et al.*, 2008). All of these models were segmented into 51 tissue types. A pregnant woman model with a gestation period of 26 weeks was also considered, taking into account 56 tissue types.

Further, a European male model named Duke and a female model named Ella were used (Christ *et al.* (2010). These models have 84 tissue types. Ar well-characterized European male model named NORMAN (Dimbylow, 1997) consisting of 37 was also employed in this study. The resolution of each model was set to 2 mm. The height, weight, surface-area-to-mass ratio, and the number of tissues for these models are summarized in Table 1.

2.2. SAR Calculation

The finite-difference time-domain (FDTD) method (Taflove and Hagness, 2003) is used for calculating the SAR in an anatomically based human model. In-house FDTD code, which was validated via intercomparison, is used (Dimbylow *et al.*, 2008). The total-field/scattered-field formulation (Taflove and Hagness, 2003) was applied in order to generate an appropriate plane wave. To incorporate the anatomically based model into the FDTD method, the electrical constants of the tissues, which depend on the frequency, are required. These values were taken from a formula based on the measurements by Gabriel *et al.* (Gabriel *et al.*, 1996). The computational region was truncated by applying a twelve-layered perfectly matched layer-absorbing boundary. For harmonically varying fields, the SAR is defined as

$$\mathrm{SAR} = \frac{\sigma}{2\rho} |\boldsymbol{E}|^2 = \frac{\sigma}{2\rho} (|\hat{E}_x|^2 + |\hat{E}_y|^2 + |\hat{E}_z|^2) \tag{1}$$

where $\hat{E}_x$, $\hat{E}_y$, and $\hat{E}_z$ are the peak values of the electric field components, and σ and ρ are the conductivity and mass density, respectively, of a tissue.

For calculating the peak spatial-averaged SAR, we considered two schemes based on the description in the IEEE standard (2002) and the ICNIRP guidelines (1998). In the scheme in IEEE (2002), the shape of the averaging volume is a cube and different tissues are allowed. The averaging scheme is not defined clearly in the ICNIRP guidelines, and any 10 g of contiguous tissue is allowed. Our algorithm to follow the ICNIRP guidelines is given in the paper of Hirata *et al.* (2006); i) voxel-SARs are sorted in the descending order, ii) the sorted voxels are divided into groups in the following manner, iii) one group is defined as a cluster of voxels, in which voxels are adjacent to each other, iv) in the descending order, a specific voxel is judged whether its sides touch existent groups. If the voxel touches no group, a new group is assigned to the voxel. If it touches exactly one group, the voxel is added to the group. When the voxel touches multiple different groups, these groups and the voxel are reclassified as a new group, v) this process is carried out to reach the mass of 10 g. As an average tissue, the skin and muscle were considered. These two schemes differ in three primary aspects: the number of tissues allowed in the averaging process, the shape of the averaging volume, and the pinna, the visible part of the ear that resides outside of the head, is considered in the average volume or not. The last factor is not crucial, as we consider whole-body exposure.

2.3. Temperature Calculation

The temperature elevation in numeric human models was calculated using the bioheat equation (Pennes, 1948). A generalized bioheat equation is given as follows:

$$C(\mathbf{r})\rho(\mathbf{r})\frac{\partial T(\mathbf{r},t)}{\partial t} = \nabla\cdot(K(\mathbf{r})\nabla T(\mathbf{r},t)) + \rho(\mathbf{r})SAR(\mathbf{r}) + A(\mathbf{r},t) - B(\mathbf{r},t)(T(\mathbf{r},t) - T_B(\mathbf{r},t)) \quad (2)$$

where $T(\mathbf{r},t)$ and $T_B(\mathbf{r},t)$ denote the temperatures of tissue and blood, respectively, C is the specific heat of tissue, K is the thermal conductivity of tissue, A is the basal metabolism per unit volume, and B is a term associated with blood perfusion.

The boundary condition between air and tissue for Eq. (2) is expressed as follows (Bernardi *et al.*, 2003):

$$-K(\mathbf{r})\frac{\partial T(\mathbf{r},t)}{\partial n} = H(\mathbf{r})\cdot(T_s(\mathbf{r},t) - T_e(t)) + SW\left(\mathbf{r},T_s(\mathbf{r},t)\right) \quad (3)$$

$$SW\left(\mathbf{r},T_s(\mathbf{r},t)\right) = P_{ins} + SW_{act}\left(\mathbf{r},T_s(\mathbf{r},t)\right) \quad (4)$$

where H, T_s, and T_e denote the heat transfer coefficient, body surface temperature, and air temperature, respectively. The heat transfer coefficient includes the convective and radiative heat losses. SW includes the heat losses due to perspiration, SW_{act}, and insensible water loss, P_{ins}. T_e is chosen as 28°C, the temperature at which thermal equilibrium is obtained in a naked man (Hardy *et al.*, 1938). The function of SW_{act} is given in our previous study (Hirata *et al.*, 2007a),

which was modified from Fiala *et al.* (2001). The perspiration coefficients are assumed to depend on the temperature elevation in the skin and/or hypothalamus:

$$SW_{act}(\mathbf{r},t) = \{W_S(\mathbf{r},t)\Delta T_S(t) + W_H(\mathbf{r},t)(T_H(t) - T_{Ho})\} / S \times 2^{(T(\mathbf{r})\text{-}T_0(\mathbf{r}))/10} \quad (5)$$

$$W_s(\mathbf{r},t) = \alpha_{11}\tanh(\beta_{11}T_s(\mathbf{r},t) - T_{so}(\mathbf{r})) - \beta_{10}) + \alpha_{10} \quad (6)$$

$$W_H(\mathbf{r},t) = \alpha_{21}\tanh(\beta_{21}T_s(\mathbf{r},t) - T_{so}(\mathbf{r})) - \beta_{20}) + \alpha_{20} \quad (7)$$

where T_S, T_H, T_{S0}, and T_{H0} are the temperatures of the skin and hypothalamus and corresponding initial temperatures, ΔT_s is the average skin temperature elevation, S is the surface area of the human body, and W_S and W_H are the weighting coefficients for perspiration rate associated with the temperature elevation in the skin and hypothalamus. Fiala *et al.* (2001) determined the coefficients of α and β for the average perspiration rate based on measurements by Stolowijk (1971); α_{10}=1.20, α_{11}=0.80, β_{10}=0.19, β_{11}=0.59, α_{20}=6.30, α_{21}=5.70, β_{20}=1.03, β_{21}=1.98.

Most thermal constants of tissues are taken from Hirata *et al.* (2008a), while those for the fetus in the pregnant woman model are taken from Kikuchi *et al.* (2010).

In order to take into account the core temperature variation in the bioheat equation, it is reasonable to consider the blood temperature as constant over the whole body and a variable of time $T_B(\mathbf{r},t) = T_B(t)$ with the initial blood temperature T_{B0} of 37°C. This assumption is often used in computational models (Fiala *et al.*, 2001) although it is not true in actual humans (Chen and Holmes, 1980). This assumption is reasonable because the *elevation* of the blood temperature from the thermoneutral condition, not the absolute blood temperature, is essential to represent the thermoregulatory response as described below, and the blood circulates throughout the human body in 1 min or less (Folkow and Neil, 1971). As is given below, the blood temperature is changed according to the following equation (Bernardi *et al.*, 2003; Hirata and Fujiwara, 2009b):

$$T_B(t) = T_{B0} + \int_t \frac{Q_{BTN}(t)}{C_B \rho_B V_B} \mathrm{d}t \quad (8)$$

where Q_{BTN} is the net rate of the heat acquisition of blood from the body tissues, C_B (=4,000 $\mathrm{Jkg^{-1}°C}$) is the specific heat, ρ_B (=1,050 $\mathrm{kgm^{-3}}$) is the mass density, and V_B is the total volume of blood. Note that the time course of core temperature can be followed reasonably even for sets of thermal parameters that do not fully get balanced when the compensation scheme of Hirata and Fujiwara (2009b) is introduced. V_B was determined as 7.5% of the weight (ICRP, 1975). The thermal constants (thermal conductivity K, specific heat C, the term associated with blood perfusion rate B, basal metabolic rate A), which depend on tissue type/organ, and the heat transfer coefficient in the human models were approximately the same as Hirata *et al.* (2008a).

If a temperature elevation was above a certain level which depends on tissue, the blood perfusion rate was increased in order to remove the excess heat evolved. Details of our thermophysiological response modeling can be found in our previous study (Hirata *et al.*,

2008a). The variation of the blood perfusion rate in the skin through vasodilatation is expressed in terms of the temperature elevation in the hypothalamus and the average temperature elevation in the skin (Bernardi *et al.*, 2003). The blood perfusion in all tissues except the skin was assumed to be governed by the local tissue temperature. When that temperature remained below 39°C (Hoque and Gandhi, 1988), blood perfusion was equal to its basal value B_0. Once the local temperature exceeded the threshold of 39°C, blood perfusion increased almost linearly with the temperature in order to remove the heat evolved. The blood perfusion model described by Bernardi *et al.* (2003) provides a higher temperature elevation than the other models (Laakso and Hirata, 2011) and is thus applied for a conservative estimation.

Perspiration for the adult is modeled on the basis of the formulas of Fiala *et al.* (2001). The perspiration coefficients are assumed to depend on the temperature elevation in the skin and the hypothalamus. The point to be stressed here is that the perspiration model for the adult was applicable even to 5–10-month-old infants when compared with the measurement for the body temperature variation and sweating in a hot environment (Hirata *et al.*, 2008a). This finding implies that the perspiration rate integrated over the body is determined by the body core and skin temperature elevations only, even for different ages and morphologies. This modeling for children, however, has been verified for the core temperature elevation of up to 0.4°C. Thus, computations of the core temperature elevation larger than this value may have some uncertainty.

The computational code taking into account the thermoregulatory response was verified by comparing the computed and measured temperatures in the skin and the body core while changing the ambient temperature (Tsuzuki-Hayakawa *et al.*, 1995). It was also verified by comparing the measured and computed temperature elevations in rabbits exposed to microwaves (Hirata *et al.*, 2008b).

2.4 Analytic Formula to estimate temperature

In order to discuss the effectiveness of core temperature elevation computed with the FDTD method, the following analytic formula is used, which was derived in our previous study (Hirata *et al.*, 2009):

$$T(t) \simeq T_0 + \frac{P}{S(H_{eff} + SW(t))}\left(1 - \exp\left(-\frac{S(H_{eff} + SW(t))}{W \cdot C_{ave}}t\right)\right) \tag{9}$$

where W is the weight of the model, P is the power absorbed in the model, C_{ave} is the mean value of the specific heat over the body [J kg^{-1} ^{o}C], and H_{eff} is the heat transfer integrated over the body surface [W ^{o}C^{-1}]. $SW(t)$ is identical to (4) except for the temperature assumed to be spatially uniform; core and skin temperature is assumed to be identical in (5).

2.5. Exposure scenario

One of the models is chosen and assumed to be standing in free space. As an incident wave, a plane wave with a vertical polarization is considered. The plane wave is incident on the human models from the front (along the anteroposterior direction). The reason for choosing this incident direction is that it results in a higher WBA-SAR compared to incident directions directly or obliquely from the sides, above, or below (Uusitupa *et al.*, 2010; Kühn *et al.*, 2009). In addition, The scenario considered here correspond to the one deriving the relationship between the basic restriction and reference level in the international guidelines/standard (ICNIRP, 1998; IEEE, 2006).

The duration of exposure was chosen as 1 hour. This duration was chosen so as to be longer than the averaging time of 30 min considered in the ICNIRP guidelines (ICNIRP, 1998) and the thermal time constant for the male with a smaller perspiration rate (40-50 min) in our previous study (Hirata *et al.*, 2007a).

3. Results

3. 1. Correlation between WBA-SAR and core temperature elevation

Figure 1 shows the WBA-SAR and core temperature elevation in TARO exposed at the reference level (ICNIRP, 1998; IEEE, 2006); 2 W m^{-2} for frequencies up to 400 MHz and $f/(2\times 10^8)$ W m^{-2} for frequencies between 400 MHz and 2 GHz, and 10 W m^{-2} for frequencies higher than 2 GHz. From figure 1, we observe that the WBA-SAR has peaks at 60 MHz (the resonance frequency) and 2 GHz, as suggested in previous studies (Dimbylow, 2002; Hirata *et al.*, 2007b; Conil *et al.*, 2008). Note that the second peak is caused by the increase of the allowable incident power density or the relaxation of the reference level with the increase of the frequency (ICNIRP, 1998; IEEE, 2006). In addition, the core temperature elevation has peaks at the same frequencies.

In order to obtain insight the above-mentioned tendency, the temperature elevation distributions at 60 MHz, 1 GHz, and 5 GHz are presented in figure 2 for WBA-SAR of 0.4 W/kg. In addition, the time evolutions of skin and core temperatures and those of blood perfusion rate in the skin and sweating rate integrated over the body are shown in figure 3. Note that the exposure duration was chosen as 2 h in this figure to confirm the thermal evolution of the temperature elevation and thermophysiological responses. As shown in figure 2, high temperature elevations are observed inside the body at 60 MHz, while the highest temperatures are concentrated around the body surface at 5 GHz. As shown in figure 3 (a), the skin temperature elevation is higher and increases quicker at 5 GHz than at 1 GHz and 60 MHz. On the contrary, the core temperature elevation becomes smaller at higher frequencies (see figure 3

(b)). At 1 h, the core temperature elevation is 83-87% of that in the thermally steady state. As shown in figure 3 (c), the sweating rate integrated over the body increases quickly at 5 GHz while the increase is somewhat slower at 60 MHz. This is because the sweating rate is governed by the temperature elevations in the skin and body core, suggesting that the former temperature elevation is dominant at 2,400 s or earlier. The blood perfusion rate in the skin averaged over the body was smaller at higher frequency because the skin temperature in the frontal side of the body only increased due to the exposure, in addition to smaller core temperature elevation (figure 3 (d)).

The core temperature elevation normalized by the WBA-SAR is shown in figure 4 for the WBA-SAR values of 0.08 Wkg^{-1}, 0.4 Wkg^{-1}, and 4 Wkg^{-1}. Note that the WBA-SAR values of 0.08 Wkg^{-1} and 0.4 Wkg^{-1} are the basic restriction or general public and occupational exposure in the international guidelines (ICNIRP, 1998; IEEE, 2006), respectively, and 4 Wkg^{-1} is the lower threshold at which the thermophysiological behavior was observed in rodents (Michaelson, 1983). In the same figure, the values estimated by our analytical formula (9) are also shown for the sake of comparison. As seen from figure 4, the ratios of the core temperature elevation to the WBA-SAR are more or less constant at frequencies lower than a few gigahertz and then gradually decrease with an increase in the frequency. This tendency was almost identical for different WBA-SAR values. The difference in the ratios obtained by the FDTD and the analytical formula was at most 10% at frequencies lower than 2 GHz.

The same measure was examined for six other human body models. As seen from figure 5, a significant difference in the core temperature elevation normalized by the WBA-SAR of 0.4 W kg^{-1} was observed between the child and the remaining adult models. Although not shown here, the computed core temperature elevation normalized by the WBA-SAR was in good agreement with that derived from our analytic formula(Hirata *et al.*, 2009), as in the case of TARO (figure 4).

3. 2. Maximum temperature elevations in the whole body normalized by peak 10-g averaged SAR

The SAR averaged over 10 g of tissue and the maximum temperature elevation in the whole body of TARO are shown in figure 6. Local SAR was normalized by the WBA-SAR of 0.4 Wkg^{-1}. For computing the local spatial-averaged SAR, we used the algorithm prescribed in the IEEE standard (2006) and that developed from the description in the ICNIRP guidelines(ICNIRP, 1998). From figure 6, we observe that the peak 10-g averaged SAR and the maximal temperature elevation depend on the frequency of the incident electromagnetic waves. The SAR computed with the ICNIRP guidelines is higher than that computed using the IEEE standard over the considered frequencies (Hirata *et al.*, 2006). For the ICNIRP averaging

scheme, the maximum temperature elevation appeared in the muscle for frequencies below 3 GHz and in the skin at frequencies higher than 3 GHz. The locations of the peak averaged SAR computed with the IEEE and ICNIRP averaging schemes were close to each other. The same tendency was observed for the WBA-SAR values of 0.08 and 4 Wkg^{-1}.

Figure 7 shows the maximum temperature elevations in TARO normalized by the peak 10-g averaged SAR at the WBA-SAR values of 0.08, 0.4, and 4 Wkg^{-1}. The maximum temperature elevation decreased when normalized by relatively high WBA-SAR values. When the WBA-SAR was 0.4 Wkg^{-1}, the maximum temperature elevation normalized by the local SAR computed with the IEEE scheme was in the range of 0.19–0.25 $°C \cdot kgW^{-1}$ at frequencies lower than 4 GHz and then gradually increased at higher frequencies. In contrast, the maximum temperature elevation normalized by the SAR computed with the ICNIRP scheme was insensitive to the frequency of the incident wave: 0.14 and 0.22 $°C \cdot kgW^{-1}$ over the considered frequencies.

The local SAR averaged over 10 g of tissue and the maximum temperature elevation in the body of TARO excluding the extremities are shown in figure 8, when normalized at the WBA-SAR of 0.4 Wkg^{-1}. Note that an additional reduction factor of 2 is applied in the extremities. For the data presented in figure 8, the maximum temperatures normalized by the local SAR are shown in figure 9. As seen from figure 9, the normalized maximum temperature elevation was in the ranges of 0.17–0.29 $°C \cdot kgW^{-1}$ for the IEEE averaging scheme and 0.13–0.24 $°C \cdot kgW^{-1}$ for the ICNIRP averaging scheme. Similar to the case including extremities, the maximum temperature elevation decreased in the case of relatively high WBA-SAR values.

The maximum temperature elevations normalized by the 10-g SAR in different body models including and excluding the extremities are shown in figures 10 and 11, respectively. The IEEE averaging scheme was used here. From these figures, it can be seen that the same tendency was observed as that for TARO. A good agreement was observed in the normalized temperature elevation of different human body models over the considered frequencies, except in the case including the extremities and above 4 GHz.

Figures 12 illustrate the positions where the peak SAR and the temperature elevation appeared for TARO and the 3-year-old child model for including (a) and excluding (b) the extremities. The WBA-SAR value of 0.4 W kg^{-1} was chosen here. In these figures, we observed that the positions where the peak SAR and the temperature elevation appeared were close to each other in most cases. When including the extremities, the peak SARs and the maximum temperature elevations appeared in the extremities, and when excluding the extremities, they appeared in the head and neck.

4. Discussion

4. 1. Comparison of our computational results with those in previous studies

In order to confirm our computational results, we compared them with those obtained by Bakker *et al.* (2011), in which the thermoregulatory response and the core temperature elevation were not considered. In the study of Bakker *et al.* (2011), the normalized maximum temperature elevation averaged over 10 to 5.6 GHz was 0.26 °C·kgW^{-1}. The corresponding value obtained herein ranged from 0.19 to 0.25 °C·kgW^{-1} for a WBA-SAR value of 0.08 Wkg^{-1} when the thermoregulatory response worked marginally. One of the reasons for this difference is that 12 exposure directions were considered and their average values were presented in the paper of Bakker *et al.* (2011) while only one direction (front to back) was considered in this study. The other reason is the difference in the thermal constants used. Note that the blood perfusion rate B in Eq. (2) is suggested to be the dominant factor affecting the local temperature elevation ((Hirata *et al.*, 2006; Samaras *et al.*, 2007b; Laakso and Hirata, 2011). The computed core temperature elevation was in good agreement with that derived from the empirical equation (Hirata *et al.*, 2009), as shown in Fig. 4. The difference of the core temperature elevation estimated using the analytic formula from the FDTD-derived results was 5% or less in the frequency from 10 to 50 MHz where the difference was the smallest, as shown in Fig. 4.

4.2. Frequency dependence of WBA-SAR and temperature elevations

The core temperature normalized by the WBA-SAR decreased gradually in the gigahertz region, as shown in figures 4 and 5. This decrease may not be explained by the analytical formula (Hirata *et al.*, 2009). For exposure duration of 1 h, the total sweating over the body of TARO was 18.5 g, 19.3 g, and 20.1 g at 60 MHz, 2 GHz, and 5 GHz, respectively, for the WBA-SAR of 0.4 W kg^{-1}, and 288 g, 289 g, and 281 g at 60 MHz, 1 GHz, and 5 GHz, respectively, for the WBA-SAR of at 4 W kg^{-1}; no clear difference is observed in the total sweating over the frequencies. Thus, one of the primary reasons for the decrease of the normalized core temperature elevation with frequency would be the increased convective and radiative heat losses due to the higher skin temperature elevation at higher frequencies (see figure 3(a)). The normalized core temperature elevation decreased with higher WBA-SAR values. This is because of the sweating. The sweating rate is governed by the average skin temperature and the core temperature (Fiala *et al.*, 2001). At a WBA-SAR value of 4 W kg^{-1}, the normalized core temperature was rather insensitive to the frequency of the incident wave. The sweating rate is mainly characterized by the core temperature elevation for this WBA-SAR, because the skin temperatures at 60 MHz, 1 GHz, and 5 GHz are –0.28 ºC, –0.05 ºC, and 0.68 ºC, respectively. Thus, the effects of convection and radiation are smaller than those at lower WBA-SAR.

The core temperature elevations normalized by the WBA-SAR in the adult models were

almost identical. As discussed in our previous studies (Hirata *et al.*, 2009; Laakso and Hirata, 2011), the body-surface-area-to-mass ratio is a dominant factor affecting this measure. As listed in Table 1, the body-surface-area-to-mass ratios are almost identical to each other in all the considered cases. There are two primary reasons for the difference in the core temperature elevations between the adult models. One is the uncertainty of the body-surface-area-to-mass ratios, which were roughly estimated from an empirical equation (Fujimoto *et al.*, 1968). The second reason is the anatomical composition of the models. Sweating is governed by the average skin temperature. However, the model resolutions of 2 mm may not be sufficient to represent the skin.

4.2. Frequency dependency of local SAR and temperature elevation

The maximum temperature elevation normalized by the peak SAR computed using the IEEE scheme became large at frequencies above 4 GHz, as shown in Fig. 7. The primary reason for this tendency is the relationship between the side length of the SAR averaging cube (~22 mm) and the penetration depth. The penetration depth of an electromagnetic wave is 6 mm at 6 GHz. Then, the averaged SAR became smaller with a decrease in the frequency. Further, the maximum temperature elevation was observed in the skin of the extremities at frequencies larger than 4 GHz. On the other hand, the maximum temperature elevation normalized by the peak SAR computed using the ICNIRP scheme did not increase at frequencies of 4 GHz or higher. When the extremities were excluded from the averaging region, the normalized maximum temperature elevation by the peak 10-g SAR was not considerably affected even at the relatively high frequencies. It was in the range of 0.17–0.29 °C·kgW^{-1} for the IEEE standard and 0.13–0.24 °C·kgW^{-1} for the ICNIRP guidelines; hence, the SAR values computed using both the averaging schemes would provide a reasonable estimate for the maximum temperature elevation. As shown in figure 7, the normalized maximum temperature elevation increased to around 60–100 MHz. The maximum temperature elevation decreased during normalization using relatively high WBA-SAR values, because of the relatively high sweating rate and increased blood perfusion as mentioned above. As illustrated in figure 11 (b), the maximum temperature elevation appeared in the muscle of the abdomen that was surrounded by fat. Then, the temperature elevation increased because of a low blood perfusion rate (Hirata *et al.*, 2006; Samaras *et al.*, 2007b; Laakso and Hirata, 2011).

The peak 10-g averaged SAR value was shown to be an appropriate metric correlating with the local temperature elevation (Hirata *et al.*, 2006; Laakso, 2009; Hirata and Fujiwara, 2009a; Razmadze *et al.*, 2009; McIntosh and Anderson, 2010). Our computational results suggested that this metric is still applicable for estimating the local temperature elevation while taking into account the thermophysiological response for WBA-SAR less than 0.4 Wkg^{-1}, as suggested by

Laakso and Hirata (2011). This tendency was confirmed for different human body models.

The local temperature elevations normalized by the local SARs computed using the IEEE scheme were not affected by the different body models. When the extremities were included, the normalized local temperature elevation in some models increased as in the case of TARO. The median value for the case including the extremities was 0.21 °C·kgW^{-1} for frequencies lower than 4 GHz, and the maximum difference was 27% (Duke at 3 GHz). The average value when the extremities were excluded was 0.19 °C·kgW^{-1} with a maximum difference of 29% (Duke at 500 GHz). The point to be stressed here is that the coefficient is close to those reported in our previous study that discussed a localized head exposure of 0.20-0.22 °C·kgW^{-1} for the IEEE averaging scheme (Hirata and Fujiwara, 2009a).

4.3. Relationship of Results and Guidelines/Standards

In the international guidelines, the safety factor of 10 is applied to the WBA-SAR value of 4 W kg^{-1} (ICNIRP, 1998; IEEE, 2006). For this WBA-SAR, the core temperature elevation is suggested to be smaller than 1-2 °C, which may induce adverse health effects such as heat exhaustion and heat stroke. From the ratio in figure 2, the core temperature elevation for WBA-SAR at 4 W kg^{-1} for 1 h duration is 0.8 °C or less. Thus the basic restriction of WBA-SAR in the international standards/guidelines is conservative at least from the standpoint of temperature elevation. This is because the basic restriction has been determined by extrapolating data from experiments using small animals and monkeys. Actually, the thermoregulatory ability in humans is far superior to that in laboratory animals (Adair and Black, 2003).

The IEEE standard changed the applicable upper frequency of WBA-SAR from 6 GHz to 3 GHz. Then, the incident power density is used as a basic restriction instead for frequencies from 3 to 300 GHz. The rationale for this change is primarily based on RF penetration depth calculations, and thus not well discussed from the standpoint of temperature elevation. In addition, it is commented that "*While the absorbed RF energy associated with exposures at high microwave frequencies is concentrated near the body's surface, resulting in localized SARs that may be substantial, the shift downward of the maximum frequency at which WBA-SAR is applicable helps emphasize a belief that the power density reference levels are extraordinarily conservative."* Let us discuss if localized SAR becomes substantial at higher frequencies as compared with WBA-SAR. The ratio of peak 10-g SAR to WBA-SAR and that of local maximum temperature elevation to core temperature elevation in TARO are shown in figure 13 (a) and (b), respectively. From figure 13 (a), the ratio of local 10-g SAR to WBA-SAR increase at frequencies from a few gigahertz, especially when including the extremity. This tendency becomes more obvious in terms of the temperature elevation, as shown in figure 13 (b), because

local temperature becomes larger (figures 6 and 8) and core temperature becomes smaller (figure 1) at frequencies higher a few gigahertz. It is noting that core temperature elevation in the child is much smaller than that of the adult (figure 5). Thus, the ratio of local maximum temperature elevation including the extremity to core elevation reached 23.5 and 63.7 at 3 GHz and 6 GHz, respectively. Core temperature elevations for exposure at the reference level of occupational exposure at 3 and 6 GHz are 0.08ºC and 0.06ºC, while those for a WBA-SAR of 0.4 W/kg are 0.12ºC and 0.10ºC, supporting the description of the IEEE standard that the power density reference levels are more conservative than the basic restriction of WBA-SAR, at least from the standpoint of the temperature elevation.

5. Conclusion

In the present study, using anatomically based human models, we computed the SAR and the temperature elevation for plane-wave exposures from 30 MHz to 6 GHz. The thermoregulatory response caused by tissue temperature elevation was taken into account in the thermal computation. Our computational results suggested that the ratio of the body core temperature to the WBA-SAR and that of the local maximum temperature to local SAR decreased with an increase in WBA-SAR because of the thermoregulatory response. For the Japanese adult male model TARO, the WBA-SAR value correlated well with the core temperature elevation for frequencies of up to a few gigahertz. At relatively high frequencies (above a few gigahertz), the core temperature elevations decreased because of increased convective and radiative heat losses from the skin to air which are attributable to the skin temperature elevation. Note that this higher skin temperature is caused by a decrease in the penetration depth. A similar tendency was observed in different human body models. In particular, core temperature elevation even for whole-body averaged SAR of 4 W kg^{-1} with the duration of 1 h was 0.8^{o}C or less. Thus, the current basic restriction for whole-body exposure in the international guidelines is conservative. In addition, our computational results support the description provided in the IEEE standard (2006) for changing the upper applicable frequency from 6 GHz to 3 GHz at least from the standpoint of the core temperature elevation; "*the shift downward of the maximum frequency at which WBA-SAR is applicable helps emphasize a belief that the power density reference levels are extraordinarily conservative"*.

The peak 10-g averaged SARs computed using the averaging schemes outlined in the IEEE standard and ICNIRP guidelines correlated well with the maximum temperature elevations over the considered frequencies even in the case of plane-wave exposures, except in the case when the extremities were included at frequencies higher than 4 GHz for the IEEE averaging scheme. Unlike the relationship between WBA-SAR and the core temperature elevation, this metric is useful or almost identical for different human body models. The coefficient characterizing their

correlation was 0.21 °C·kgW^{-1} and 0.19 °C·kgW^{-1} for the human models including and excluding the extremities, respectively. These coefficient values were close to those reported in our previous study that discussed a localized head exposure (Hirata and Fujiwara, 2009a), suggesting that the local spatial-averaged SAR, which is a metric for localized exposure, is still useful for estimating the maximum temperature elevation even for a whole-body exposure at least from 30 MHz to 6 GHz.

Additional computations and discussion are needed when discussing the product safety including magnetic resonance equipment, because the heat transfer between the body and equipment is different from the human in free space (Samaras *et al.*, 2007a).

Acknowledgement

This research was supported by Strategic International Cooperative Program (Joint Research Type), Japan Science and Technology Agency and the France National Research Agency. Ilkka Laakso wishes to thank the Academy of Finland and the Finnish Cultural Foundation for financial support.

FIGURE AND TABLE CAPTIONS

Figure 1. Whole-body-averaged SAR and core temperature elevation in Japanese male model for plane-wave exposure at the reference levels for general public.

Figure 2. Temperature elevation distributions in in Japanese male model TARO at (a) 60 MHz, (b) 1 GHz, and (c) 5 GHz.

Figure 3. Time evolution of (a) mean skin temperature elevation, (b) core temperature elevation, (c) sweating rate, and (d) normalized blood perfusion rate in the skin. Whole-body averaged SAR is 0.4 W kg^{-1}.

Figure 4. Normalized core temperature elevation in Japanese male model TARO for whole-body-averaged SARs of 0.08, 0.4, and 4 Wkg^{-1}. Estimated values using analytical formula (Hirata *et al.*, 2009) are also shown.

Figure 5. Normalized core temperature elevation by whole-body-averaged SAR in different human body models (whole-body-averaged SAR of 0.4 Wkg^{-1}).

Figure 6. Peak 10-g averaged SAR and maximum temperature elevations in the whole body of TARO at whole-body-averaged SAR of 0.4 Wkg^{-1}. Two different averaging schemes, based on the IEEE standard and ICNIRP guidelines, for peak-averaged SARs are considered.

Figure 7. Maximum temperature elevations in the whole body of TARO normalized by peak 10-g averaged SAR for different whole-body-averaged SARs. Peak 10-g averaged SAR values are calculated on the basis of the IEEE standard (cubic volume) and ICNIRP guidelines (contiguous).

Figure 8. Peak 10-g averaged SAR and maximum temperature elevations in TARO excluding the extremities at whole-body-averaged SAR of 0.4 Wkg^{-1}. Peak 10-g averaged SAR values are calculated on the basis of the IEEE standard and ICNIRP guidelines.

Figure 9. Maximum temperature elevations in TARO excluding the extremities normalized by peak 10-g averaged SAR for whole-body-averaged SARs of 0.08, 0.4, and 4 Wkg^{-1}.

Figure 10. Maximum temperature elevations normalized by peak 10-g averaged SAR in different human models (whole-body-averaged SAR of 0.4 Wkg^{-1}).

Figure 11. Maximum temperature elevations in the body excluding the extremities normalized by peak 10-g averaged SAR in different human models (whole-body-averaged SAR of 0.4 Wkg^{-1}).

Figure 12. Positions where peak 10-g averaged SAR and maximum temperature elevation appeared in TARO and 3-year-old child model: the extremities were (a) included and (b) excluded. The averaging scheme outlined in the IEEE standard was used. The black and red marks correspond to the positions of the peak SAR and maximum temperature elevation, respectively. Resonance frequencies of TARO and the 3-year-old child are 60 and 134 MHz, respectively.

Figure 11. (a) Ratio of peak SAR averaged over 10-g of tissue to whole-body-averaged SAR and (b) that of maximum temperature elevations to core temperature elevation for the cases including and excluding the extremity.

Table 1 Height, weight, body-surface-area-to-mass ratio, and number of tissues for seven human body models.

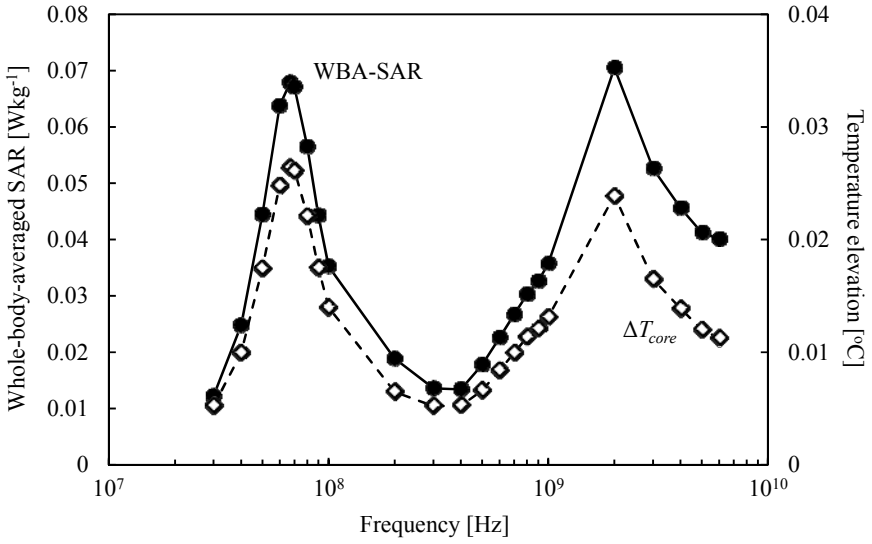
0.08
0.07
0.06
0.05
0.04
0.03
0.02
0.01
0
0.04
0.03
0.02
0.01
0
WBA-SAR
ΔT_{core}
Whole-body-averaged SAR [Wkg^{-1}]
Temperature elevation [°C]
10^7
10^8
10^9
10^{10}
Frequency [Hz]

Fig. 1.

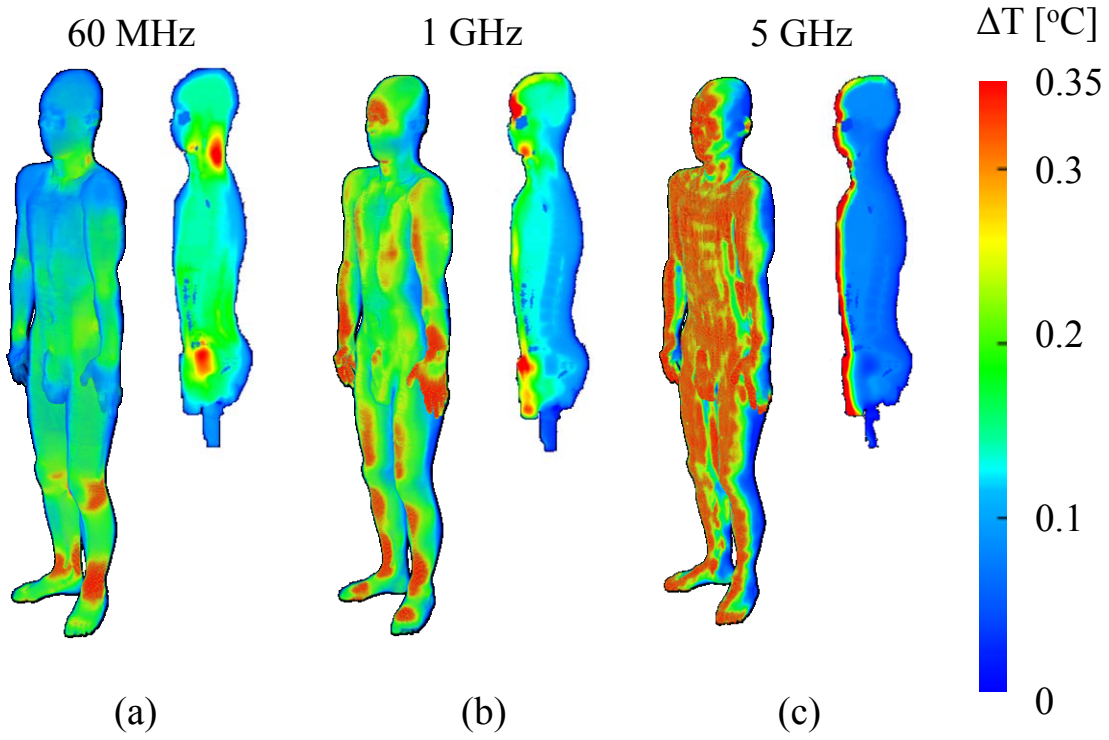
60 MHz
1 GHz
5 GHz
ΔT [°C]
0.35
0.3
0.2
0.1
0
(a)
(b)
(c)

Fig. 2

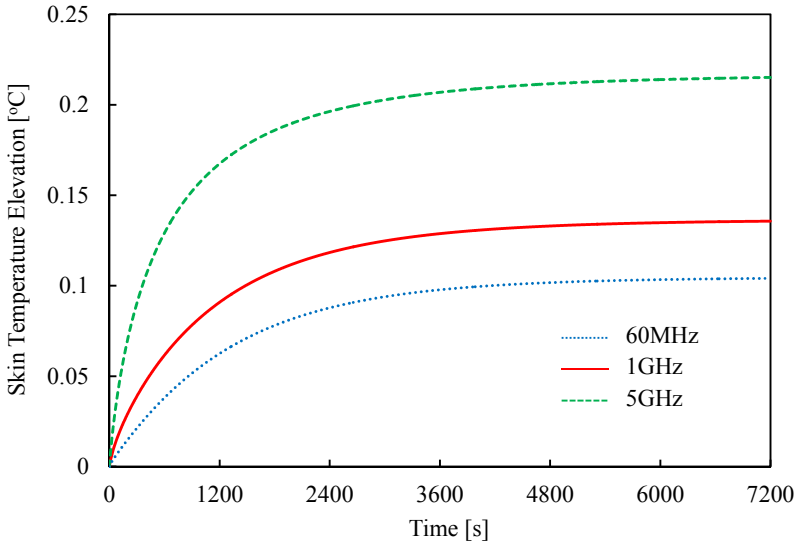
Skin Temperature Elevation [°C]
0.25
0.2
0.15
0.1
0.05
0
0
1200
2400
3600
4800
6000
7200
Time [s]
60MHz
1GHz
5GHz

(a)

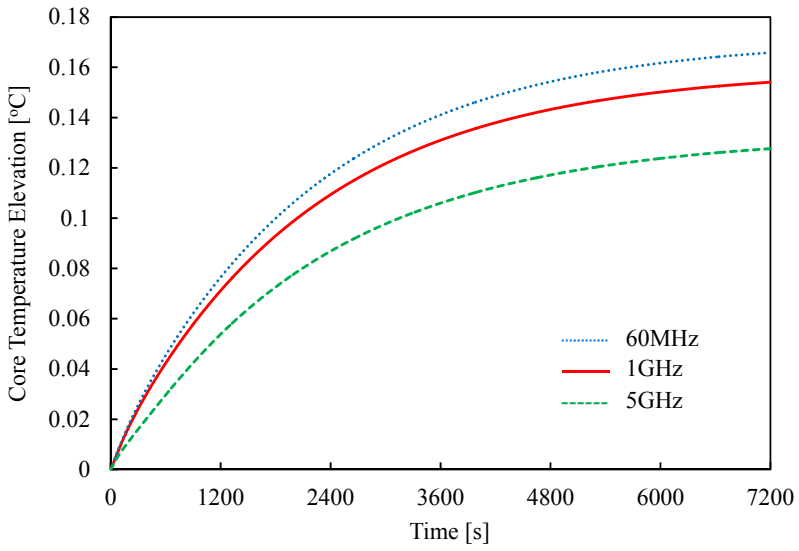
Core Temperature Elevation [°C]
0.18
0.16
0.14
0.12
0.1
0.08
0.06
0.04
0.02
0
0
1200
2400
3600
4800
6000
7200
Time [s]
60MHz
1GHz
5GHz

(b)

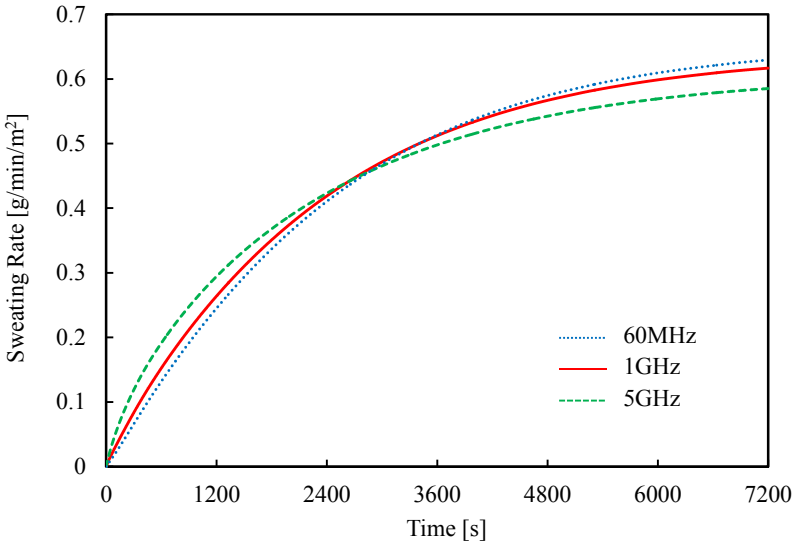
0.7
0.6
0.5
0.4
0.3
0.2
0.1
0
Sweating Rate [g/min/m²]
0
1200
2400
3600
4800
6000
7200
Time [s]
60MHz
1GHz
5GHz

(c)

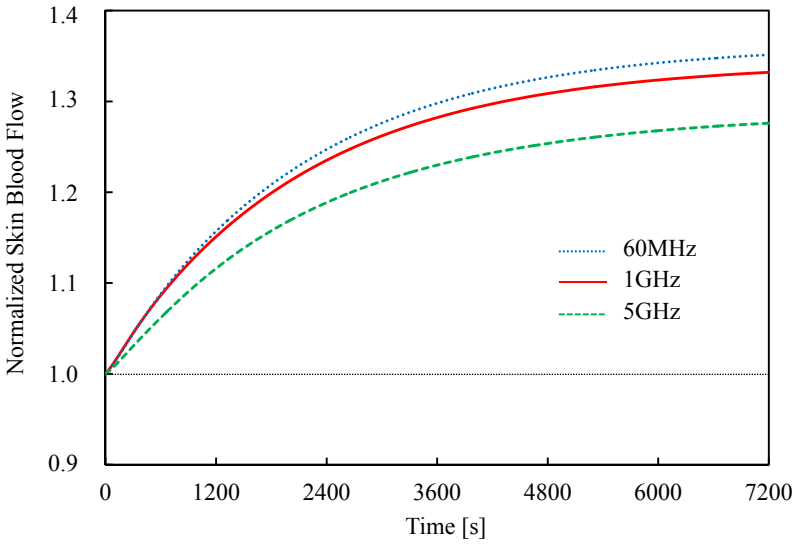
1.4
1.3
1.2
1.1
1.0
0.9
Normalized Skin Blood Flow
0
1200
2400
3600
4800
6000
7200
Time [s]
60MHz
1GHz
5GHz

(d)

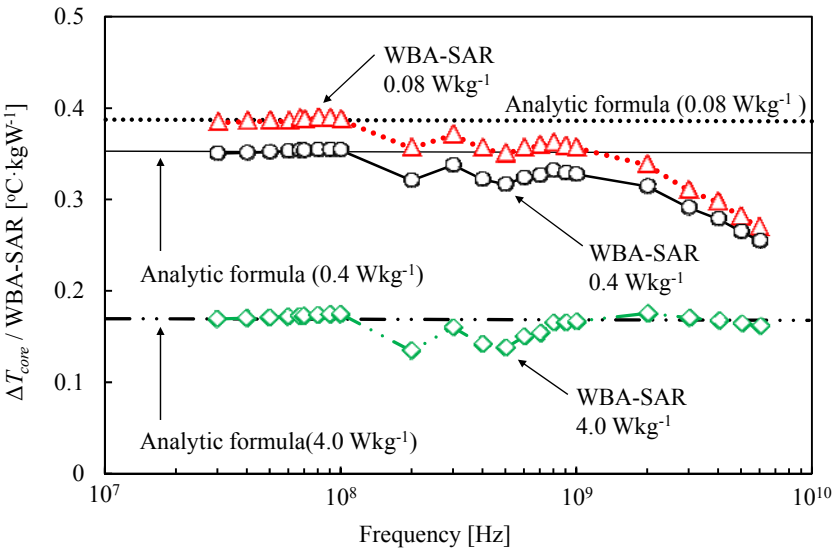
0.5
0.4
0.3
0.2
0.1
0
ΔT_{core} / WBA-SAR [°C·kgW^{-1}]
WBA-SAR
0.08 Wkg^{-1}
Analytic formula (0.08 Wkg^{-1})
Analytic formula (0.4 Wkg^{-1})
WBA-SAR
0.4 Wkg^{-1}
WBA-SAR
4.0 Wkg^{-1}
Analytic formula(4.0 Wkg^{-1})
10^7
10^8
10^9
10^{10}
Frequency [Hz]

Fig. 4.

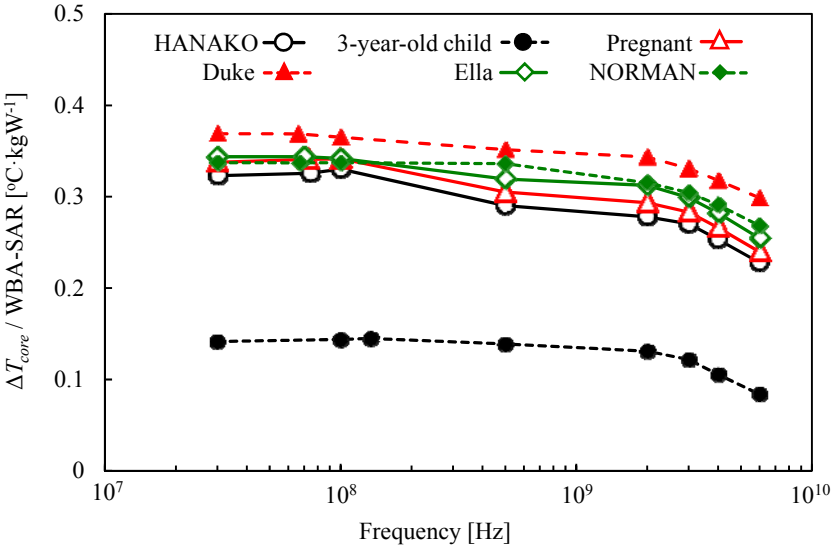
0.5
0.4
0.3
0.2
0.1
0
ΔT_{core} / WBA-SAR [°C·kgW^{-1}]
HANAKO
3-year-old child
Pregnant
Duke
Ella
NORMAN
10^7
10^8
10^9
10^{10}
Frequency [Hz]

Fig. 5.

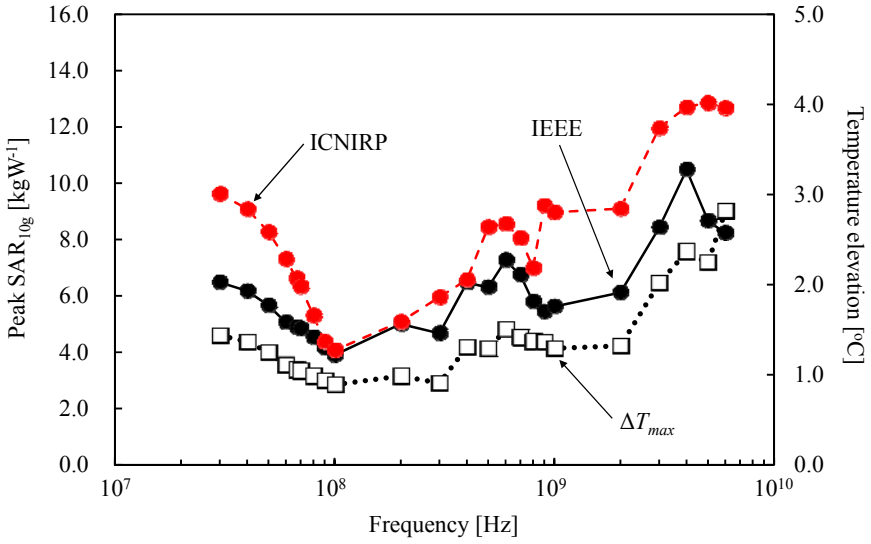
16.0
14.0
12.0
10.0
8.0
6.0
4.0
2.0
0.0
5.0
4.0
3.0
2.0
1.0
0.0
ICNIRP
IEEE
ΔT_{max}
Peak SAR$_{10g}$ [kgW^{-1}]
Temperature elevation [°C]
10^7
10^8
10^9
10^{10}
Frequency [Hz]

Fig. 6.

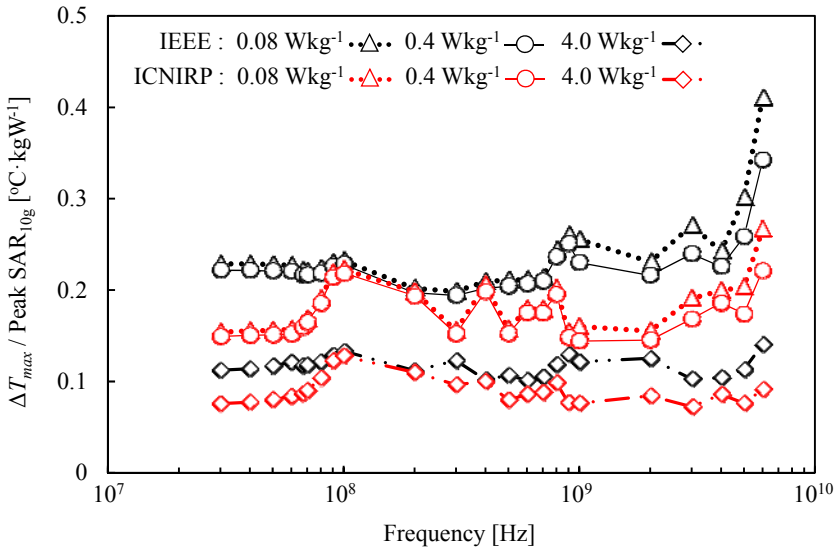
IEEE : 0.08 Wkg^{-1} 0.4 Wkg^{-1} 4.0 Wkg^{-1}
ICNIRP : 0.08 Wkg^{-1} 0.4 Wkg^{-1} 4.0 Wkg^{-1}
0.5
0.4
0.3
0.2
0.1
0
ΔT_{max} / Peak SAR$_{10g}$ [°C·kgW^{-1}]
10^7
10^8
10^9
10^{10}
Frequency [Hz]

Fig. 7.

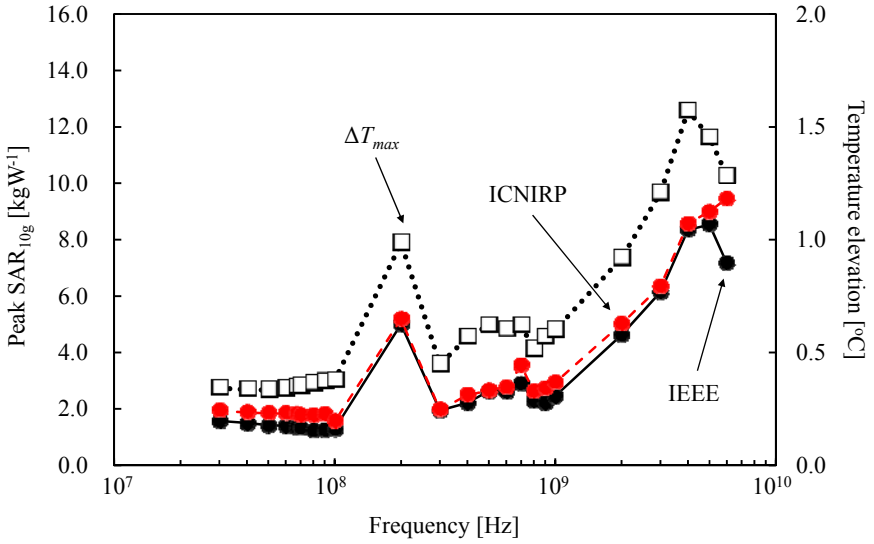
16.0
14.0
12.0
10.0
8.0
6.0
4.0
2.0
0.0
Peak SAR10g [kgW-1]
2.0
1.5
1.0
0.5
0.0
Temperature elevation [ºC]
ΔTmax
ICNIRP
IEEE
10^7
10^8
10^9
10^10
Frequency [Hz]

Fig. 8.

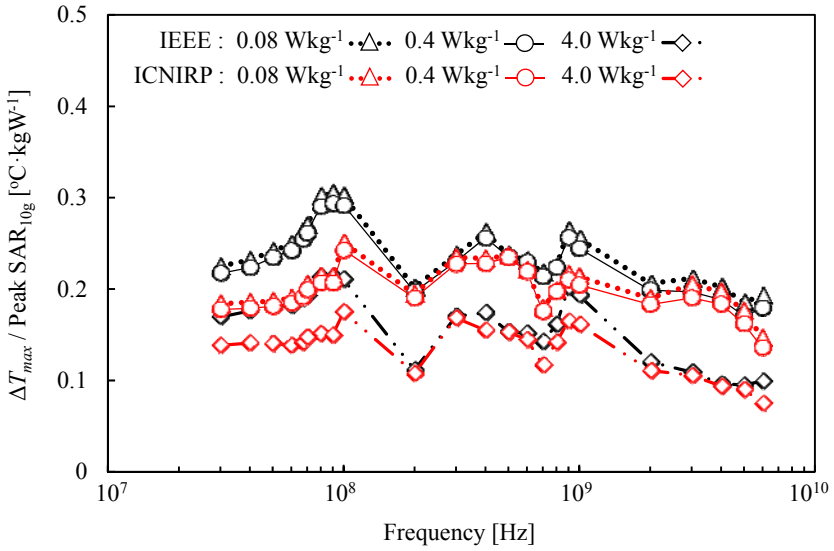
IEEE : 0.08 Wkg-1 0.4 Wkg-1 4.0 Wkg-1
ICNIRP : 0.08 Wkg-1 0.4 Wkg-1 4.0 Wkg-1
0.5
0.4
0.3
0.2
0.1
0
ΔTmax / Peak SAR10g [ºC·kgW-1]
10^7
10^8
10^9
10^10
Frequency [Hz]

Fig. 9.

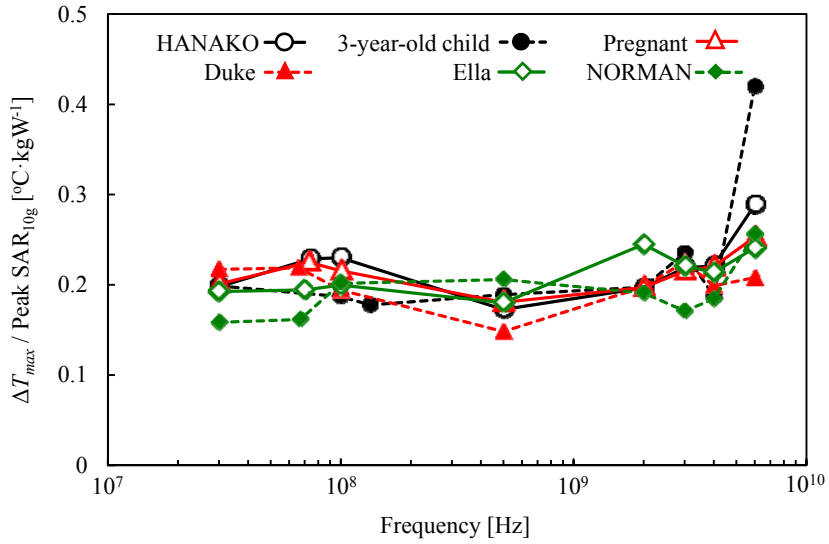
HANAKO
3-year-old child
Pregnant
Duke
Ella
NORMAN
0.5
0.4
0.3
0.2
0.1
0
ΔT_{max} / Peak SAR_{10g} [°C·kgW^{-1}]
10^7
10^8
10^9
10^{10}
Frequency [Hz]

Fig. 10.

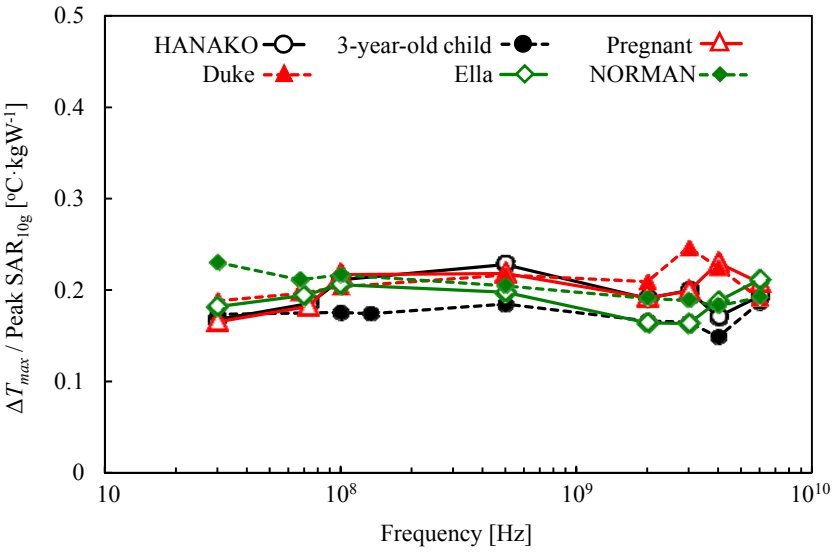
HANAKO
3-year-old child
Pregnant
Duke
Ella
NORMAN
0.5
0.4
0.3
0.2
0.1
0
ΔT_{max} / Peak SAR_{10g} [°C·kgW^{-1}]
10
10^8
10^9
10^{10}
Frequency [Hz]

Fig. 11.

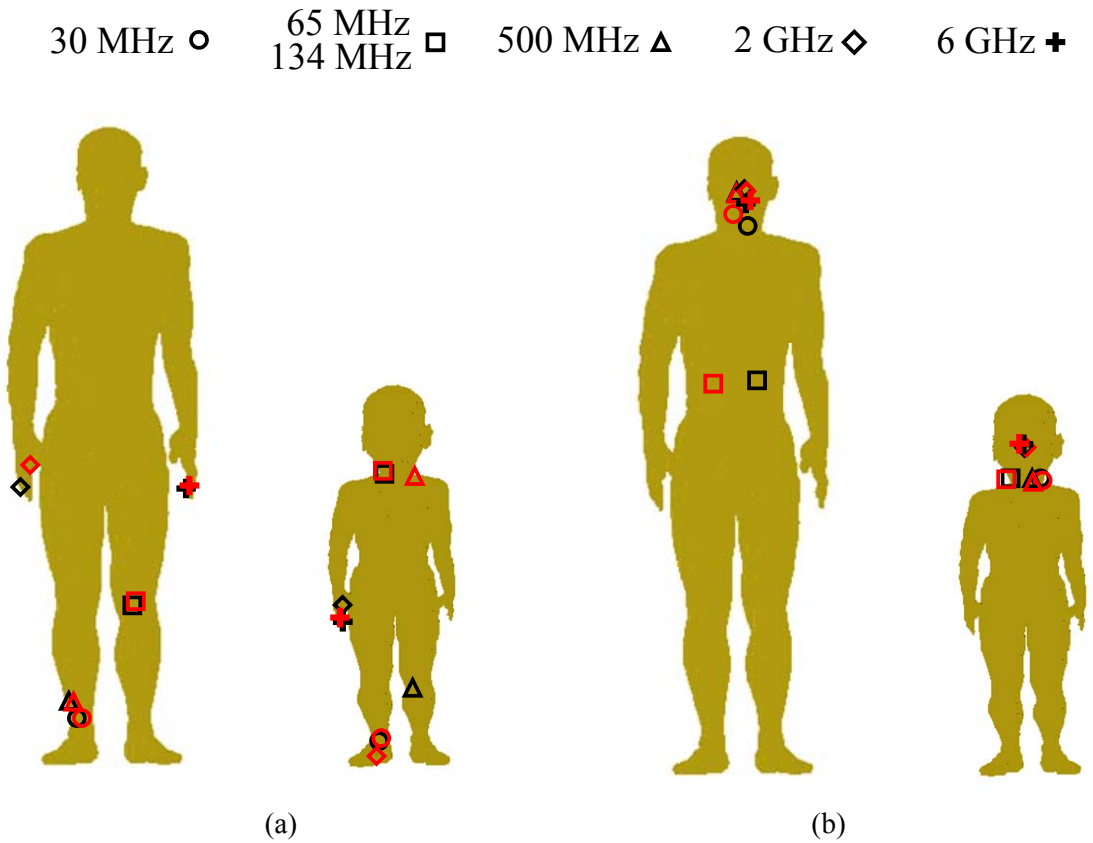
30 MHz
65 MHz
134 MHz
500 MHz
2 GHz
6 GHz
(a)
(b)

Fig. 12.

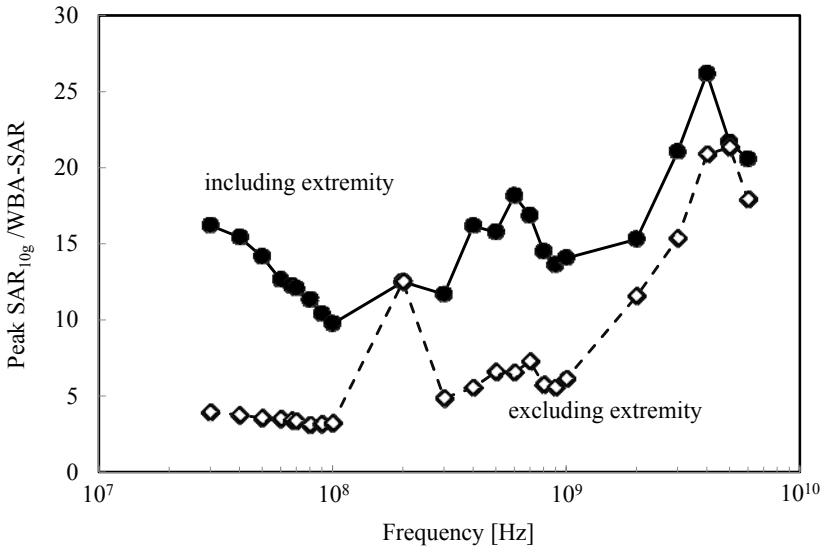
30
25
20
15
10
5
0
Peak SAR10g /WBA-SAR
including extremity
excluding extremity
10^7
10^8
10^9
10^10
Frequency [Hz]

(a)

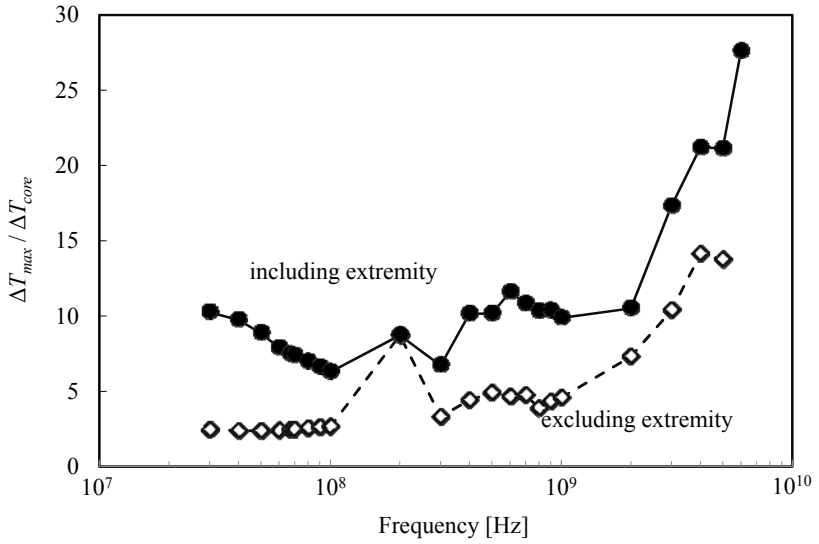

(b)

Fig. 13

Table 1

Model	TARO	HANAKO	3-year-old child	Pregnant woman	Duke	Ella	NORMAN
Height [m]	1.73	1.61	0.90	1.61	1.74	1.60	1.76
Weight [kg]	65	53	13	58	70	58	76
Surface-area-to-mass ratio[m^2kg^{-1}]	0.027	0.029	0.043	0.028	0.026	0.028	0.025
Number of tissue	51	51	51	56	84	84	37

References

ACGIH 1996 Threshold limit values for chemical substances and physical agents and biological exposure indices (Cincinnati OH

Adair E R and Black D R 2003 Thermoregulatory responses to RF energy absorption *Bioelectromagnetics* **24** S17-S38

Bakker J F, Paulides M M, Neufeld E, Christ A, Kuster N and Rhoon G C v 2011 Children and adults exposed to electromagnetic fields at the ICNIRP reference levels: theoretical assessment of the induced peak temperature increase *Phys. Med. Biol.* **56** 4967

Bernardi P, Cavagnaro M, Pisa S and Piuzzi E 2003 Specific absorption rate and temperature elevation in a subject exposed in the far-field of radio-frequency sources operating in the 10-900-MHz range *IEEE Trans. Biomed. Eng.* **50** 295-304

Chen M M and Holmes K R 1980 Microvascular contributions in tissue heat transfer *Annals of the New York Academy of Sciences* **335** 137-50

Christ A, Kainz W, Hahn E G, Honegger K, Zefferer M, Neufeld E, Rascher W, Janka R, Bautz W, Chen J, Kiefer B, Schmitt P, Hollenbach H-P, Shen J, Oberle M, Szczerba D, Kam A, Guag J W and Kuster N 2010 The Virtual Family—development of surface-based anatomical models of two adults and two children for dosimetric simulations *Physics in Medicine and Biology* **55** N23

Conil E, Hadjem A, Lacroux F, Wong M F and Wiart J 2008 Variability analysis of SAR from 20 MHz to 2.4 GHz for different adult and child models using finite-difference time-domain *Phys. Med. Biol.* **53** 1511-25

Dimbylow P J 1997 FDTD calculations of the whole-body averaged SAR in an anatomically realistic voxel model of the human body from 1 MHz to 1 GHz *Phys. Med. Biol.* **42** 479-90

Dimbylow P J 2002 Fine resolution calculations of SAR in the human body for frequencies up to 3 GHz *Physics in Medicine and Biology* **47** 2835-46

Dimbylow P J, Hirata A and Nagaoka T 2008 Intercomparison of whole-body averaged SAR in European and Japanese voxel phantoms *Phys. Med. Biol.* **53** 5883-97

Fiala D, Lomas K J and Stohrer M 2001 Computer prediction of human thermoregulatory and temperature responses to a wide range of environmental conditions *International Journal of Biometeorology* **45** 143-59

Folkow B and Neil E 1971 *Circulation* (New York: Oxford University Press)

Foster K R and Adair E R 2004 Modeling thermal responses in human subjects following extended exposure to radiofrequency energy *Biomed. Eng. Online* **3**

Fujimoto S, Watanabe T, Sakamoto A, Yukawa K and Morimoto K 1968 Studies on the physical surface area of Japanese. 18. Calculation formulas in three stages over all ages *Japanese Journal of Hygiene* **23** 443-50

Gabriel S, Lau R W and Gabriel C 1996 The dielectric properties of biological tissues: III. Parametric models for the dielectric spectrum of tissues *Phys. Med. Biol.* **41** 2271

Hardy J D, Du Bois E F and Soderstrom G F 1938 Basal metabolism, radiation, convection and vaporization at temperatures of 22 to 35°C *The Journal of Nutrition* **15** 477-97

Hirata A, Asano T and Fujiwara O 2007a FDTD analysis of human body-core temperature elevation due to RF far-field energy prescribed in the ICNIRP guidelines *Phys. Med. Biol.* **52** 5013-23

Hirata A, Asano T and Fujiwara O 2008a FDTD analysis of body-core temperature elevation in children and adults for whole-body exposure *Phys. Med. Biol.* **53** 5223-38

Hirata A, Fujimoto M, Asano T, Wang J, Fujiwara O and Shiozawa T 2006 Correlation between maximum temperature increase and peak SAR with different average schemes and masses *IEEE Transactions on Electromagnetic Compatibility* **48** 569-77

Hirata A and Fujiwara O 2009a The correlation between mass-averaged SAR and temperature elevation in the human head model exposed to RF near-fields from 1 to 6 GHz *Phys. Med. Biol.* **54** 7227-38

Hirata A and Fujiwara O 2009b Modeling time variation of blood temperature in a bioheat equation and its application to temperature analysis due to RF exposure *Phys. Med. Biol.* **54** N189-N96

Hirata A, Kodera S, Wang J and Fujiwara O 2007b Dominant factors influencing whole-body average SAR due to far-field exposure in whole-body resonance frequency and GHz regions *Bioelectromagnet.* **28** 484-7

Hirata A, Sugiyama H and Fujiwara O 2009 Estimation of core temperature elevation in humans and animals for whole-body averaged SAR *Prog. in Electromagnetics Res.* **99** 53-70

Hirata A, Sugiyama H, Kojima M, Kawai H, Yamashiro Y, Fujiwara O, Watanabe S and Sasaki K 2008b Computational model for calculating body-core temperature elevation in rabbits due to whole-body exposure at 2.45 GHz *Phys. Med. Biol.* **53** 3391-404

Hoque M and Gandhi O P 1988 Temperature distributions in the human leg for VLF-VHF exposures at the ANSI-recommended safety levels *Biomedical Engineering, IEEE Transactions on* **35** 442-9

ICNIRP 1998 Guidelines for limiting exposure to time-varying electric, magnetic, and

electromagnetic fields (up to 300 GHz) *Health Phys.* **74** 494-521

ICRP 1975 *Report of the Task Group on Reference Man* vol 23 (Oxford, UK: Pergamon Press)

IEEE 2002 *IEEE Standard for Safety Levels with Respect to Human Exposure to Electromagnetic Fields, 0 to 3 KHz*

IEEE 2006 IEEE standard for safety levels with respect to human exposure to radio frequency electromagnetic fields, 3 kHz to 300 GHz *IEEE C95.1*

Kühn S, Jennings W, Christ A and Kuster N 2009 Assessment of induced radio-frequency electromagnetic fields in various anatomical human body models *Physics in Medicine and Biology* **54** 875

Kikuchi S, Saito K, Takahashi M and Ito K 2010 Temperature elevation in the fetus from electromagnetic exposure during magnetic resonance imaging *Physics in Medicine and Biology* **55** 2411

Laakso I 2009 Assessment of the computational uncertainty of temperature rise and SAR in the eyes and brain under far-field exposure from 1 to 10 GHz *Physics in Medicine and Biology* **54** 3393

Laakso I and Hirata A 2011 Dominant factors affecting temperature rise in simulations of human thermoregulation during RF exposure *Phys. Med. Biol.* **56** 7449

McIntosh R L and Anderson V 2010 SAR versus Sinc: What is the appropriate RF exposure metric in the range 1–10 GHz? Part II: Using complex human body models *Bioelectromagnetics* **31** 467-78

Michaelson S M 1983 Biological effects and health hazards of RF and MW energy: Fundamentals and overall phenomenology *Biological Effects and Dosimetry of Nonionizing Radiation* 337-57

Nagaoka T, Kunieda E and Watanabe S 2008 Proportion-corrected scaled voxel models for Japanese children and their application to the numerical dosimetry of specific absorption rate for frequencies from 30 MHz to 3 GHz *Phys. Med. Biol.* **53** 6695-711

Nagaoka T, Watanabe S, Sakurai K, Kunieda E, Taki M and Yamanaka Y 2004 Development of realistic high-resolution whole-body voxel models of Japanese adult males and females of average height and weight, and application of models to radio-frequency electromagnetic-field dosimetry *Phys. Med. Biol.* **49** 1-15

Pennes H H 1948 Analysis of tissue and arterial blood temperatures in the resting human forearm *J. Appl. Physiol.* **1** 93-122

Poljak D, Tham C Y, Gandhi O and Sarolic A 2003 Human equivalent antenna model for transient electromagnetic radiation exposure *IEEE Transactions on Electromagnetic Compatibility* **45** 141-5

Razmadze A, Shoshiashvili L, Kakulia D, Zaridze R, Bit-Babik G and Faraone A 2009 Influence of Specific Absorption Rate Averaging Schemes on Correlation between Mass-Averaged Specific Absorption Rate and Temperature Rise *Electromagnetics* **29** 77-90

Samaras T, Christ A, Klingenbock A and Kuster N 2007a Worst Case Temperature Rise in a One-Dimensional Tissue Model Exposed to Radiofrequency Radiation *Biomedical Engineering, IEEE Transactions on* **54** 492-6

Samaras T, Kalampaliki E and Sahalos J N 2007b Influence of Thermophysiological Parameters on the Calculations of Temperature Rise in the Head of Mobile Phone Users *Electromagnetic Compatibility, IEEE Transactions on* **49** 936-9

Taflove A and Hagness S 2003 Computational Electrodynamics: The Finite-Difference Time-Domain Method. 3rd Ed.

Tsuzuki-Hayakawa K, Tochihara Y and Ohnaka T 1995 Thermoregulation during heat exposure of young children compared to their mothers *European Journal of Applied Physiology and Occupational Physiology* **72** 12-7

Uusitupa T, Laakso I, Ilvonen S and Nikoskinen K 2010 SAR variation study from 300 to 5000 MHz for 15 voxel models including different postures *Physics in Medicine and Biology* **55** 1157

Ziskin M C and Morrissey J 2011 Thermal thresholds for teratogenicity, reproduction, and development *International Journal of Hyperthermia* **27** 374-87